Properties of Medium Hydrogenated Béryllium Nanoparticles

Alexandros G. Chronis, Michael M Sigalasa, François Virot, Marc Barrachin, Emmanuel . Koukaras, Aristides Zdetsis

Properties of Medium Hydrogenated Beryllium Nanoparticles

Alexandros G. Chronis[a], Michael M. Sigalas[a], François Virot[b], Marc Barrachin[b], Emmanuel N. Koukaras[c], Aristides D. Zdetsis[d]

[a]*Department of Materials Science, University of Patras, 26504 Patras, Greece*
[b]*Institut de Radioprotection et de Sûreté Nucléaire PSN-RES, SAM, Saint Paul les Durance cedex 13115, France*
[c] *Laboratory of Quantum and Computational Chemistry, Department of Chemistry, Aristotle University of Thessaloniki, GR-54124 Thessaloniki, Greece*
[d]*Molecular Engineering Laboratory, Department of Physics, University of Patras, 26500, Greece*

Abstract

The dust concern in ITER fusion facility calls for improvement of the knowledge of their fundamental properties because important safety issues are associated with them; including radiological hazard, toxicity as well as chemical reactivity in terms of explosion risks. Additional risk related to the particle class of nanometric size has to be futhermore consider due to their impact on biological environment since their production in fusion facility has been put in evidence. Specifically, although no data has been acquired on beryllium nanoparticles (NPs) and their reactivity within tritium, the aim of this present paper is to establish a first comprehensive picture of beryllium–hydrogen based nanoparticles. The structural and electronic properties of Be_n and Be_nH_m NPs of "medium" sizes are investigated using Density Functional Theory calculations. Starting from bare NPs to find the relevant nanoparticle shape, the insertion sites of hydrogen are then identified and characterized. Finally, our study focusses on the highly hydrogenated particles which are studied and the relative stability trends are established.

Keywords: Nanoparticle, hydrogen, beryllium, ITER

1. Introduction

Beryllium (and tungtsen) has been selected as the first-wall (divertor) material for the International Thermonuclear Experimental Reactor (ITER), the world's largest magnetic fusion device, that will be fueled by deuterium and tritium. There are some concerns on the effects resulting from the impact of energetic particles on the plasma-faced surfaces such as mechanical degradation of armoring materials and production of dust. The first predictive amount of generated dust has been performed by Shimada *et al.*[1], whereas their impacts on tokamak safety has been recently presented by Grisolia *et al.*[2]. Although the dust has received little attention within the fusion community (mainly because dust was neither a safety nor an operational problem in existing tokamaks), the ITER design has highlighted the fundamental need to deepen understanding of the dust behaviour. This is because dust behaviour is associated to important safety issues which include radiological hazard (tritium and activation products), toxicity (beryllium), and chemical reactivity with steam and air. In situations of air and/or water ingress in the vacuum vessel, an important contributor to potential release could be expected [3] to be activated dust that can be put in resuspension, and transported through the different compartiments of the installation. Such dust could be theoretically composed of tritium, beryllium, tungsten, and activation corrosion products present in the coolant loop (in case of water ingress). This paper is mainly focussed on the behaviour of such particles, and more precisely on the tritium behaviour in beryllium particles in terms of insertion and desorption energies.

Such physical processes have been extensively studied at the atomic scale in bulk beryllium [4–10]. The most recent calculations give indications that hydrogen solubility in beryllium is favoured by the presence of vacancies but remains in any case relatively low, in agrement with experimental data. In the case of defect-free beryllium, hydrogen diffuses by a succession of jumps between the basal tetrahedral (BT) and octahedral (O) sites with an activation barrier of 0.39 eV. The investigated multi-trapping process showed that the introduction of several hydrogen atoms into a vacancy is ener-

Email address: sigalas@upatras.gr (Michael M. Sigalas)

getically favourable up to five atoms and had to be considered in the mechanisms of hydrogen retention and desorption in beryllium.

Very few data are available regarding the interaction between hydrogen isotopes and particles. The structural properties of particles are expected to differ significantly from their bulk counterparts. Factors that contribute to such differences may be induced by structural strains or change in reactivity, due to much larger surface to volume ratios. It is expected that these differences are also reflected in the interaction between the dust and the hydrogen isotopes.

Past-studies experimental [11, 12] as well as theoretical [13–19] have been devoted to interaction between hydrogen and beryllium surfaces. A large number of these studies was limited to the investigation of the (0001) basal plane, calculated to be the most stable surface [17], the energies of the prismatic and pyramidal surfaces being slightly higher. First-principles recent calculations [16] put in evidence that there are no molecular adsorption states for H_2 on the basal plane. The lowest dissociation energy barrier is 0.75 eV for adsorbing H_2. The diffusion energy barrier is rather small, $\approx$ 0.35 eV, while the penetration energy barrier is much larger, $\approx$ 1.25 eV, so the dissociated H atoms are expected to diffuse around on the Be(0001) surface without penetrating into the subsurface sites. Stumpf *et al.*[13] established that at lower hydrogen coverages, the hcp hollow site is energetically more favorable, while hydrogen at the fcc site has a slightly higher energy, consistently with the recent DFT calculations [17]. Finally, another study of hcp beryllium has examined the effect of hydrogen surface coverage on surface energy and relaxation of outermost atomic layers [18]. Multiscale simulations were performed by Stihl *et al.*[19] which associated DFT calculations, a cluster expansion method to approximate the energies of arbitrary hydrogen adsorption configuration, and a kinetic Monte Carlo method for dynamic simulations, capture the overall trends of the deuterium coverage behaviour onto a beryllium surface. In a more recent study [20], using similar multiscale simulations the hydrogen isotope desorption from (0001) beryllium surface was calculated as well as the co-adsorbed hydrogen isotopes in the immediate vicinity of the desorbing pair.

The structure of beryllium nanoparticles and their hydrides have been recently studied by Zdetsis *et al.*[21]. In this work, they have thoroughly and systematically determined the structural, cohesive, and electronic properties of Be_n and Be_nH_{xn} ($n = 2 - 160$, $x = 0.1 - 2.4$) nanoparticles as a function of both size (n) and hydrogen content (x), using Density Functional Theory (DFT) with different functionals. Results benchmarked against high accuracy coupled-cluster CCSD(T) lead to select the hybrid meta-GGA M06 functional as the most accurate one. Also for both beryllium and beryllium hydride, the M06 functional used with the cc-pVTZ basis set have been shown to be able to reproduce, for very large clusters, the experimental and the DFT values of the bulk cohesive energy, respectively. They predicted that most of the structures corresponding to the lowest energy stoichiometric Be_nH_{2n} nanoparticles are chains or chain-like structures. The tendency towards chain stabilization of Be_nH_{xn} nanoparticles increases, as x approaches the stoichiometric value $x = 2$, leading for large values of n, to polymeric forms of bulk BeH_2, which in the past have been considered as the structures preferred by solid BeH_2 [22–26]. More recently, Koukaras *et al.*[27] confirmed these results by the study of fully hydrogenated beryllium nanoclusters of Be_nH_{2n} ($n = 3 - 20$) generic compositions, using DFT and the M06 functional and CCSD(T). For small nanoclusters (n≤9), the lowest energy geometry has linear or polymeric form while for larger nanoclusters, calculations confirm that ring structures are energetically more favorable. In addition to the binding energies of the structures Koukaras *et al.*report on polymerization energies, Be−H bond energies with respect to coordination details, hydrogen desorption energies of saturated and oversaturated species.

In the present study, structural and cohesive characteristics (geometries, binding energies and desorption energies) of nanostructured Be_n and Be_nH_m have been examined with suitable DFT calculations, focusing on the reactivity of hydrogen within Be nanoparticles (NPs) of "medium" sizes ($\approx$ 2 nm). All obtained structural and energetic data can be used in the future to establish a dataset able to extend the existing beryllium−hydrogen interatomic potential (for molecular dynamic codes) to study the nanoparticles. After a brief description of the computational approach (section 2), the results of the DFT calculations are presented in section 3. Finally, some conclusions are drawn in section 4.

2. Computational techniques

Computations within the DFT and the generalized-gradient approximation (GGA) were performed. Firstly, the DMol tool [28] was employed for the geometry optimizations, using the PBE functional [29]. The optimizations were performed with coarser criteria and then with tighter criteria, in order to achieve the best possible energy. As for the coarser criteria, the DN ba-

sis set [30] was used and as for the convergence tolerance, the energy was set to 10^{-4} Ha, the maximal force at 0.02 Ha/Å and the maximal displacement to 0.05 Å. For more accurate results, the tighter criteria use the DND basis set [30] and as for the convergence tolerance, the energy was set to 10^{-5} Ha, force at 0.004 Ha/Å and the displacement to 0.005 Å. Also, the DIIS size was set to 10 and the smearing parameter to 0.005 Ha. Secondly, single point calculations were performed using the TURBOMOLE program [31], for all the optimized structures. The functional was again PBE, while the basis set was def-SV(P) [32], since they found to offer good agreement when compared to results from higher level of theory on similar type of NPs of smaller sizes [21, 27]. The convergence criterion was set to 10^{-6} and the DIIS to 10. Also thermodynamic temperature broadening [31] was used to help convergence. Two approaches have been used for the construction of the Be_n NP structures (Figure 1). The first nanoparticle shape is obtained by performing a spherical cut into bulk beryllium crystal whereas the second one is based on equilibrium shape of NP using the Wulff construction [33]. Regarding the latter, the NP input structure files are computed within the support of MPinterface python package [34], whereas the energies of any beryllium bare surfaces are taken from Ref. [18]. The variation of hydrogen covered energy surfaces is not taken into account to build the initial NP structures. In regard of Wulff NP, main part of this work has been performed within NP diameter of ≈1.6 nm (Be_{318}) (sphere including all beryllium atoms) whereas some additional calculations have been performed with NP of ≈2.1 nm (Be_{588}). Regarding the insertion of hydrogen atoms, for any cases ten different configurations were considered to identify the lowest energy or energetically low structures.

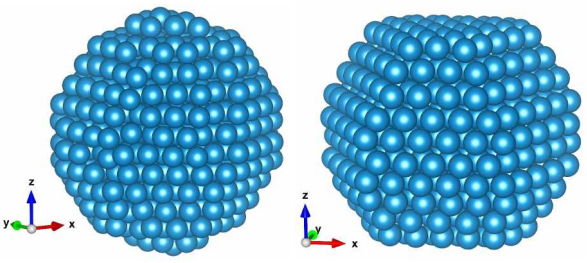

Figure 1: An illustration of the Be_{588} nanoparticules built using the spherical cut (left) and the Wulff polyhedron method (right). the basal surfaces (0001) are normal to z-axis.

3. DFT results

3.1. Bare Be NPs

Experimentally, there are no published data about the structural properties of beryllium nanoparticles, nevertheless the beryllium bond lengths trend can be compared with avaivalable bulk data. Comparison of pair distribution functions shows no significant difference of nearest neighbors compared to theoretical bulk data independently of the shape of nanoparticle (Figure 2). Therefore the finite size constraints do not affect the beryllium crystal structure. Regarding to the spherical nanoparticle, dispersion is higher due to a more significant surface reconstruction than one obtained by Wulff polyhedron method. In addition, results state present computational approach is reliable one due to agreement with recent theoretical data [9] themselves in agreement with experimental data in terms of beryllium bond lengths near NP core. At the vicinity of NP surface, nonetheless bond lengths are tightly relaxed (dispersion to dashed line of pair distribution functions in Figure 2) but there is no major distorsion of beryllium bond lengths.

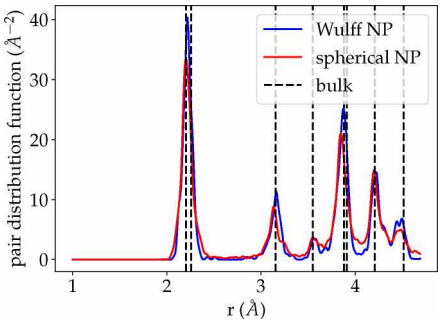

Figure 2: Part of pair distribution functions of Be_{588} for two different NP shapes. Location of dashed lines are extracted from optimized cell of Ref. [9]. Pair distribution function is computed with Diffpy tool [35].

The trend of cohesive energy for both NP shapes is shown in Figure 3. As expected, the two facetted NPs are more stable than ones obtained from spherical cut method because the former are obtained by minimizing the surface energy. But it is also clear that the original geometry is important for (and can biased) the geometry optimization, since the process cannot escape the local minima. In addition, with spherical cuts it is not always possible to construct NPs of a given total number without creating additional broken bonds and isolated atoms violating the overall symmetry. Nonetheless the

spherical cuts method is ideal when the total number of atoms is not fixed and can be determined by symmetry and topological considerations [21]. However, indepen-

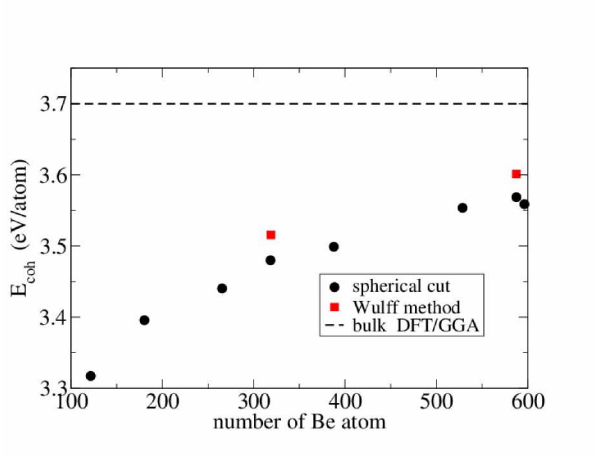

Figure 3: The cohesive or binding energy of the Be_n NP. Bulk data is taken in Ref. [9].

dently of the NPs shape, the cohesive energy is rising as the number of beryllium increasing and tends towards the bulk theoretical value for a big NP.

3.2. Hydrogenated Be nanoparticles

3.2.1. $Be_{318}H$ NPs

From the most stable structure of bare Be_{318} structure obtained by the Wulff approach, the stability of hydrogen insertion is investigated from surface to core with special attention to ridge and surface states. The aim is to identify the strongest interaction sites for a single hydrogen atom. In this case the process is described by the following reaction:

$$Be_{318}^{bare} + \frac{1}{2}H_2 \rightarrow Be_{318}H \qquad (1)$$

which characterizes the adsorption energy in case of ridge/surface sites or to the insertion energy in core structure cases.

Figure 4 shows all stable sites of hydrogen found in Be_{318} NPs where labelling F, H and S corresponds to surface sites and R denoted the ridge sites. The labels L, and M correspond to octahedral-like and basal tetrahedral-like bulk (core) sites, respectively. For exemple, L4 is located at the center of NP. Due to the effect of finite size system, induced relaxation could lead to missleading comparisons with beryllium slab results [17], especially regarding to the lateral surface sites (in respect of basal plane). Nevertheless for the adsorption

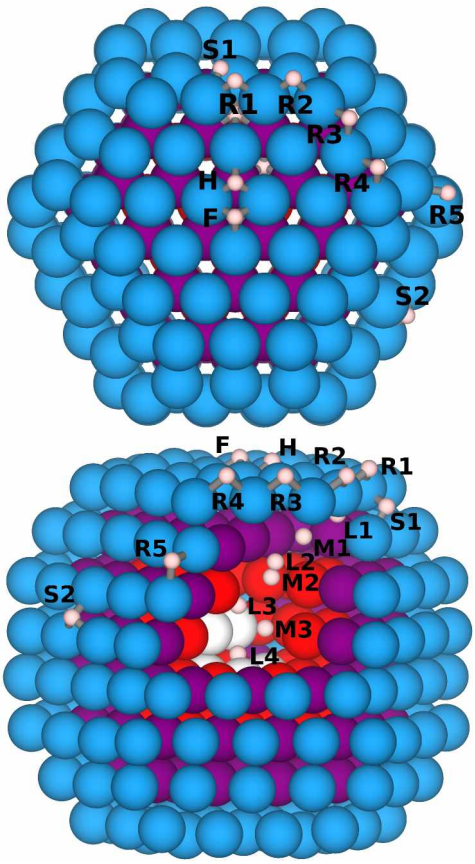

Figure 4: $Be_{318}H$ nanoparticles : investigated sites (beige spheres) of hydrogen at top, lateral and ridge of NP as well as towards the core of NP (some atoms has been removed to show NP interior). Colors correspond to layers of NP from surface (blue) to core (white). Top layer is (0001) plane.

sites into the basal plane some similarities can be highlighted. As expected, hollow sites are stable whereas bridge and atop are unstable. The F site corresponds to hollow fcc for which the bond length Be−H is 1.56 Å. On the other hand, in the H site which appear to be a hollow hcp, the three-fold axis is in fact "broken" leading to bond lengths equal to 1.55 and 1.6 Å. Moreover, the relative stabilities found here are in agreement with experiment [36]. The adsorption into ridge states is always as bridge-like bond (top site is not stable) with shorten Be−H bond lengths (<1.5 Å). On the other hand, the investigated lateral surface sites S1 and S2 sites are in fact the same absorption site but the beside surface differs. Formally, these sites are onto the $(1\bar{1}01)$-like surface, therefore they are roughly similar to the ones obtained from slab calculations [17] but the crosscheck cannot be extend so for due to the small particle size.

The corresponding energy landscape of investigated hydrogen sites is shown in Figure 5. Firstly, the insertion energies increase as the hydrogen atom is moving away from the top layer to the core of NP. The process becomes unfavourable once hydrogen inserts in sites L1 to L4, in which the energy is gradually rising as it approaches the particle center. As in beryllium bulk case, the basal tetrahedral-like site (Figure 5) are most stable than its adjacent octahedral-like ones. Nonetheless due to finite size structure, energy profiles are asymmetric which confirms that even at center of NPs the bulk behaviour is not reached. This is firstly confirmed by the noticeable difference between the insertion energies in NP center, 1.37 eV, versus bulk ones (1.67 eV in BT site and 1.87 eV for O one in Ref. [10]) which may be potentially explained by the small nanoparticle diameter. Secondly, a recent slab calculation of hydrogen diffusion from (0001) surface shows a similar energetic trend in which the influence of surface has been enabled for a deeper distance [20]. Nevertheless, a contribution due to different computational approaches cannot be excluded.

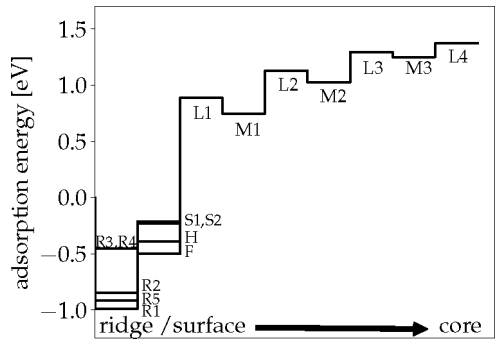

Figure 5: Energy landscape of the adsorption (formation) energies of hydrogen in $Be_{318}H$. The location label corresponds to ones shown in Fig. 4. Each steps correspond to stable hydrogen insertion sites.

Moving the hydrogen atom along the outer surface of particle leads to negative adsorption energy in a range of −0.23 to −0.99 eV. The more negative the value is, the more strongly the hydrogen atom is bound to the beryllium atoms. Hydrogen ridge bindings are stronger due to the smaller number of Be atoms at those sites. In contrast, the subsurface location (L1) is already unfavourable with an absorption energy equals to +0.89 eV. This significant energy rise can be explained by a low beryllium bond distortion in this area in comparison to the particle core (see previous section).

To summurize, the ridge sites are the most favourable trapping locations for hydrogen with strong bonds while the hydrogen is less bound into surface site. These results suggest that only the outer of NPs leads to negative formation energies, whereas a gap to positive value can be observed once hydrogen penetrates in the subsurface. Based on the results shown in Figure 5 we should expect that the hydrogen coverage of actual NPs will follow the energetical trend.

3.2.2. $Be_{318}H_m$ and $Be_{588}H_m$ NPs

We can now proceed to the discussion of the behaviour of NPs with a significant amount of hydrogen on the basis of the knowledge of formation energies of hydrogen in $Be_{318}H$. Regarding $Be_{318}H_m$, the most favourable sites (see Fig. 5) are gradually filled as m is increasing from 30 atoms up to 180 atoms (Fig. 6). In the latter, even if the ratio H/Be is high (≈0.6), hydrogens remain located at the NP surface. In this case a quasi-complete coverage of the nanoparticle is reached. Insertion inside NP has been examined but the corresponding stabilities were much lower in accordance with the findings of previous section. Indeed, ridge sites are filled first while the lateral surface sites are then occupied when m is rising. Same approach is applied to $Be_{588}H_m$ for two different hydrogen amounts : 50 and 100 atoms (not shown).

The hydrogen desoprtion energy (per one H atom) is calculated as following:

$$E_d = \frac{1}{m}\left(E(Be_n^{bare}) + \frac{m}{2} \times E(H_2) - E(Be_nH_m)\right) \quad (2)$$

where n is the number of beryllium atoms and m is the number of hydrogen atoms. Desorption energy, which corresponds to the required energy to form gaseous molecular hydrogen (hypothetically) and bare NP is shown in Figure 7. In case of $Be_{318}H_m$, the desorption energy is linearly decreasing as m is increasing nonetheless it remains positive even at quasi-fully coverage (m = 180) which indicates that highly hydrogenated nanoparticles are stable (the zero-point energy as well as the temperature effect are neglected in this study). Similar —roughly linear —trends for desorption of adsorption with respect to surface coverage have been shown by beryllium slab computations (for different surface orientations) in which hydrogen coverage varied [18].

The desorption energy trend shows that the formation of molecular hydrogen is not favourable and the hydrogen's interaction energy is always weakly repulsive in the investiguated $Be_{318}H_m$ configurations. For the con-

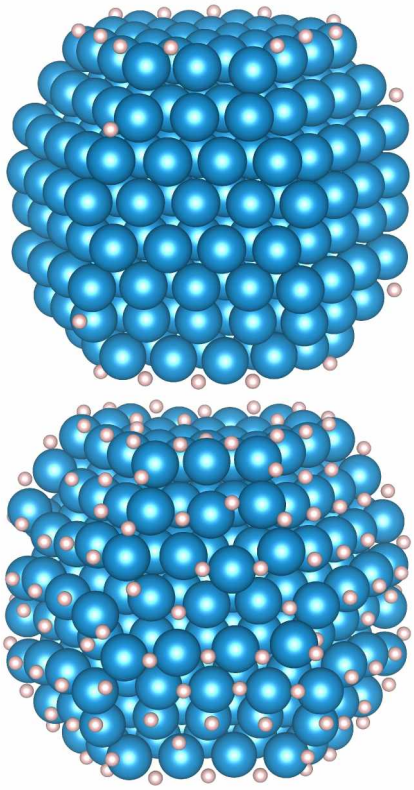

Figure 6: Example of $Be_{318}H_m$ nanoparticles for the extremum investigated cases ($m = 30$ and $m = 180$). Blue (beige) spheres correspond to beryllium (hydrogen) atoms. Hydrogen locations are chosen from study on $Be_{318}H$ (previous section).

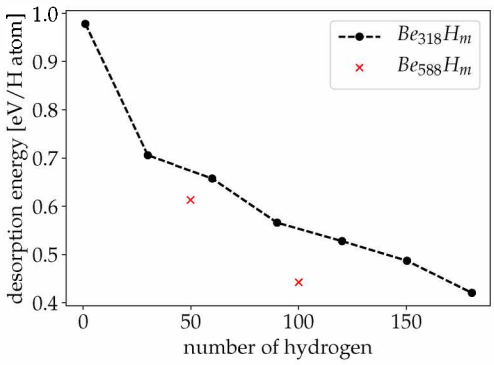

Figure 7: Evolution of desorption energy per hydrogen atom for the $Be_{318}H_m$ NP in function of number of hydrogen. Investigated $Be_{588}H_m$ cases are also shown. The case $m = 1$ corresponds to the energy of a hydrogen atom at the R1 site.

figuration where $m = 30$, the most favourable configuration (drawn in Fig. 6), in which R5 sites are filled to the detriment of R3 ones, is in accordance with energy landscape (Fig. 5). Nonetheless to illustrate the configuration effect, the hydrogen ring decoration (filled R3 sites rather than R5) has been computed. As expected the obtained desorption energy is lower (0.67 eV/H atom). These values, shown in Fig. 7, are comparable to the tendencies obtained on medium sized Be−H clusters by Zdetsis *et al.*[21]. Also, in these previous calculations it was found that the desorption energies tend to decrease as the number of hydrogen atom increases. A similar trend has been found in our current calculations. Finally, as in our previous calculations, for low concentrations of hydrogen, the H atoms prefer to be located in the surface of the nanoparticle, between two Be atoms. Two additional calculations have been made within a bigger NP ($Be_{588}H_{50}$ and $Be_{588}H_{100}$), these structures exhibit a weaker hydrogen stability. According to Eq. 2, the formation energy can be expressed as $E_f = -m \times E_d$ by considering the reference state for beryllium is that of bare nanoparticle. Therefore the present results suggest that the hydrogenated beryllium nanoparticle can be energetically stable up to high H/Be value due to significant surface/volume ratio of small NP. Our results seem to agree with the corresponding findings of Peillon *et al.*for the case of tungsten dusk [37].

4. Conclusions

The present results for medium nanoparticles confirm, as expected, that facetted nanoparticles are more stable than ones with spherical arrangement because the former minimizes the number of broken bonds. The investigations on hydrogen insertion behaviour on Be_{318} state that ridges are the most favourable adsorption sites with negative formation energies, while absorption energy becomes immediately unfavourable once hydrogen penetrates in sub-surface where the formation energy tends to bulk values, corresponding to hydrogen concentrated towards NP center. The established energy landscape has been then used to investigate the stability of highly hydrogenated nanoparticles. These results indicate that desorption energy remains positive even at full coverage due to negative adsorption energy, as well as weak hydrogen−hydrogen interaction. Results indicate that desorption energy remains positive even at full coverage due to negative adsorption energy as well as weak hydrogen−hydrogen interaction.

All these DFT data with respect to the hydrogen behaviour onto and into NP will be used in future works as energy dataset for optimization of a beryllium−hydrogen interatomic potential. This improvement would facilitate molecular dynamics simu-

lations in a wide range of cases related to hydrogen reactivity with beryllium nanoparticle, as for example the desorption temperature of hydrogen isotopes or their agglomeration and adhesion mechanisms. Molecular dynamics simulations will permit also the investigation of more representative (realistic) sizes of nanoparticles up to ≈ 10 nm.

References

[1] M. Shimada et al. *J. Nucl. Mater.*, 438:S996, 2013.
[2] Ch. Grisolia et al. *Nucl. Fusion*, 59:086061, 2019.
[3] F. Virot, L. Ferry, Y. Ferro, C. Pardanaud, and M. Barrachin. *Fusion Eng. Des.*, 124:1171, 2017.
[4] M.G. Ganchenkova and V.A. Borodin. *Phys. Rev. B*, 75:054108, 2007.
[5] S.C. Middleburgh and R.W. Grimes. *Acta Mater.*, 59:7095, 2011.
[6] M.G. Ganchenkova, V.A. Borodin, and R.M. Nieminen. *Phys. Rev. B*, 79:134101, 2009.
[7] M.G. Ganchenkova, P.V. Vladimirov, and V.A. Borodin. *J. Nucl. Mater.*, 386:79, 2009.
[8] P. Zhang, J. Zhao, and B. Wen. *J. Phys. Condens. Mat.*, 24:095004, 2012.
[9] L. Ferry et al. *Nucl. Mater. Ener.*, 12, 453 2017.
[10] L. Ferry et al. *J. Nucl. Mater.*, 524:323, 2019.
[11] K. Pohl and E.W. Plummer. *Phys. Rev. B*, 59:R5324, 1999.
[12] K. Pohl, E. Ward Plummer, Soren V. Hoffmann, and Ph. Hofmann. *Phys. Rev. B*, 70:235424, 2004.
[13] R. Stumpf and P.J. Feibelman. *Phys. Rev.B*, 51:13748, 1995.
[14] R. Stumpf. *Phys. Rev. B*, 53:4253, 1996.
[15] A. Allouche. *Phys. Rev. B*, 78:085429, 2008.
[16] Y. Li, Y. Yang, B. Sun, Y. Wei, and P. Zhang. *Physics Letters A*, 375:2430, 2011.
[17] D.V. Bachurin and P.V. Vladimirov. *Surf. Sci.*, 641:198, 2015.
[18] D.V. Bachurin and P.V. Vladimirov. *Acta Mater.*, 134:81, 2017.
[19] Ch. Stihl and P.V. Vladimirov. *Nucl. Mater. Ener.*, 9:547, 2016.
[20] Ch. Stihl, P.V. Vladimirov, and A. Moslang. *J. Nucl. Mater.*, 543:152595, 2021.
[21] A.D. Zdetsis, M.M. Sigalas, and E.N. Koukaras. *Phys. Chem. Chem. Phys.*, 16:14172, 2014.
[22] G.E. Coates and F. Glockling. *J. Chem. Soc.*, page 2526, 1954.
[23] E.L. Head, C.E. Holley, and S.W. Rabideau. *J. Am. Chem. Soc.*, 79:3687, 1957.
[24] R.W. Baker et al. *J. Organomet. Chem.*, 159:123, 1978.
[25] G.J. Brendel, E.M. Marlett, and L. M. Niebylski. *Inor. Chem.*, 17(12):3589, 1978.
[26] Tj. Tague and L. Andrews. *J. Am. Chem. Soc.*, 115:12111, 1993.
[27] E.N. Koukaras, A.P. Sgouros, and M.M. Sigalas. *J. Am. Chem. Soc.*, 138:3218, 2016.
[28] B. Delley. Dmol, a standard tool for density functional calculations: Review and advances. In *Modern Density Functional Theory*, volume 2, page 221. Elsevier, 1995.
[29] J.P. Perdew, K. Burke, and M. Ernzerhof. *Phys. Rev. Lett.*, 77(18):3865, 1996.
[30] B. Delley. *J. Chem. Phys.*, 92:508, 1990.
[31] TURBOMOLE V7.2 2017, a development of University of Karlsruhe and Forschungszentrum Karlsruhe GmbH, 1989-2007, TURBOMOLE GmbH, since 2007; available from `http://www.turbomole.com`.
[32] F. Weigend and R. Ahlrichs. *Phys. Chem. Chem. Phys.*, 7:3297–3305, 2005.
[33] G.D. Barmparis, Z. Lodziana, N. Lopez, and I.N. Remediakis. *Beilstein, J. Nanotechnol.*, 6:361, 2014.
[34] M. Kiran et al. *Comp. Mat. Sci.*, 122:183, 2016.
[35] P. Juhás, C. L. Farrow, X. Yang, K. R. Knox, and S. Billinge. *Acta Crystallogr. A*, 71:562, 2015.
[36] R. Kolasinski and J. A. Whaley. Hydrogen binding configuration and desorption kinetics on beryllium and tungsten surfaces, 2014. https://www.osti.gov/servlets/purl/1126895.
[37] S. Peillon, G. Dougniaux, M. Payet, E. Bernard, G. Pieters, S. Feuillastre, S. Garcia-Argote, F. Gensdarmes, C. Arnas, F. Miserque, N. Herlin-Boime, C. Grisolia, and Pluchery O. *Nucl. Mater. Ener.*, 24:100781, 2020.